PHYSICSAccess Research Paper
ISSN Online: 2756-3898, ISSN Print: 2714-500X https://doi.org/10.47514/phyaccess.2024.4.2.015

Investigating the Impact of Voltage on Optoelectronic Features of Silver Incorporated into the Lattice of Zirconium Sulphide Nanostructured Material

Shaka O Samuel[1], Ernest O Ojegu[2] and Imosobomeh L Ikhioya[3, 4]

[1] Department of Science Laboratory Technology, Delta State University, Abraka, Delta State, Nigeria
[2] Department of Physics, Delta State University, Abraka. Delta State, Nigeria
[3] Department of Physics, Federal University Lokoja, Kogi State, Nigeria
[4] Department of Physics and Astronomy, University of Nigeria, Nsukka, 410001, Enugu State, Nigeria

Corresponding E-mail: imosobomeh.ikhioya@unn.edu.ng

Received 02-11-2024
Accepted for publication 25-11-2024
Published 26-11-2024

Abstract

This research aims to enhance the optoelectronic properties of Ag-doped ZrS through electrochemical deposition. Different characterization techniques were employed to examine the optical, structural, and morphological properties of the synthesized material, with results showing that the absorbance of ZrS and Ag-doped ZrS changes with the applied voltage, enhancing carrier concentration and mobility at higher voltages to enhance absorption properties. ZrS displays a bandgap energy of 2.00 eV, showing its potential as a semiconductor material, while Ag-doped ZrS results in higher bandgap energies between 2.15 eV and 2.50 eV, leading to modifications in its electronic characteristics. The crystal planes of 101, 103, 111, and 112 are identified by precise 2θ angles of 23.59°, 34.91°, 48.42°, and 62.62° for ZrS and 19.64°, 33.61°, 44.48°, and 63.31° for Ag-doped ZrS. Altering voltages (10, 12, 14 V) affect the electrical structure in XRD analysis, influencing peak positions and intensities. A more evenly distributed Ag layer, preserving surface smoothness, results from lowering the voltage while introducing Ag. The interaction of Ag and ZrS leads to localized structural changes. As the voltage increases, the surface roughness of Ag-doped ZrS increases more than the undoped ZrS. The resistivity values decrease as the voltage increases, suggesting enhanced conduction and more charge carriers. The increased conductivity values (4.34, 4.58, 4.71 and 4.78 S/m) indicate that higher voltage enhances conductivity, benefiting applications needing efficient charge transfer.

Keywords: Nanostructure; silver, zirconium; bandgap; deposition; voltage.

I. INTRODUCTION

Energy storage devices have become vital as renewable energy sources become more prevalent and place greater demands on the grid infrastructure. To tackle these crucial problems, we need affordable and eco-friendly materials for harvesting and energy storage [1]–[4]. Nanostructures have attracted considerable attention from researchers due to their

synthesis, characterizations, and wide-ranging applications. The properties of these nanostructures differed from their bulk properties. The properties of nanostructured materials, such as nanotube nanocrystals and nanoribbons depend on their structures, morphologies and sizes. The focus of materials scientists is on developing innovative means of fabricating nano-sized materials with specific properties [5], [6]. Adjusting the size of nanomaterials allows for significant control over their properties, making them ideal for electron transistors, spintronics, LEDs, solar cells, quantum dot lasers, and optoelectronics [7]–[9]. One of their fundamental properties is how the bandgap energy depends on the nanocrystal size when smaller than the Bohr exciton radius.

The research community has been highly interested in nanosized structures due to their exceptional physical, chemical, mechanical, and electrical properties in recent years. Nanostructured components can boost the efficiency of solar panels and hydrogen fuel cells, meeting the rising energy demands. Utilizing renewable resources is an eco-friendly way to reduce CO_2 emissions, a growing concern today [10]. The past decade has witnessed a significant increase in interest in these materials, driven by the intriguing changes in electrical, optical, and magnetic properties as the material transitions from a solid to a particle comprising atoms. Recent progress in synthesizing and studying functional nanostructured materials highlights the unique physics and chemistry that emerges when electrons are confined in nanoscale semiconductors and metal clusters and colloids [11]. The role of carbon-based nanomaterials and nanostructures, such as fullerenes and nanotubes, is becoming increasingly significant in nanoscale science and technology.

The information age heavily relies on optoelectronic materials for its technologies. Thin-film transistors, light-emitting diodes, solar cells, sensors, and quantum-information systems all utilize them. Advances in semiconductor growth processes brought about the discovery of recent phenomena and exponential growth in technological applications. Researchers harnessed quantum confinement effects to achieve control over energy levels and densities of states in semiconductor nanostructures like quantum dots and quantum wells. These revolutionary progressions altered almost every dimension of present-day existence [12]. Despite the ongoing dominance of growth processes, there is an emergence of new synthetic approaches and device process approaches that offer the potential for lower cost and less energy-intensive fabrication of complex functional materials and devices while allowing targeted molecular designs for desired properties [10]–[14].

Silver (Ag) doped zirconium sulfide (ZrS) has received a lot of attention in materials research because of its potential qualities for a variety of applications, such as optoelectronics, photonics, and solid-state devices. ZrS, a wide bandgap semiconductor, has unique optical and electrical properties that can be increased by doping. The addition of Ag, a transition metal to the ZrS lattice, can alter its structural, electrical, and optical properties, enhancing its performance in technological applications [15]. Dopants such as Ag can affect the carrier concentration, mobility, and overall conductivity of a material. This is significant for applications in electrical devices that require efficient charge transmission. The capacity to tune these features through controlled doping opens the door to the development of innovative materials that fulfil the needs of modern technology [16], [17]. The structural properties of Ag-doped ZrS have been widely investigated. According to research [18-19], including Ag in the ZrS lattice can alter the lattice characteristics and crystallinity. Studies utilizing X-ray diffraction (XRD) have demonstrated that adding Ag causes a modest expansion of the lattice, which can be attributed to Ag's greater ionic radius than Zr. This structural alteration is important because it can affect the material's electrical characteristics. The electrical characteristics of Ag-doped ZrS have been the focus of investigation [18], [19]. Doping with Ag has been shown to greatly increase the conductivity of ZrS. Studies have shown that altering Ag concentrations between 0.01 and 0.05 mol can optimize carrier concentration, resulting in increased electrical performance [15], [19]. The mechanisms underlying this increase frequently involve the formation of extra charge carriers and enhanced mobility due to reduced scattering. The optical characteristics of Ag-doped ZrS are also quite interesting, especially for photonic applications [20]. Research [19]-[21], has shown that Ag doping can affect ZrS's bandgap, making it appropriate for specific optical applications. Photoluminescence investigations show that Ag-doped samples have higher luminescence qualities than undoped ZrS [19]. This boost is ascribed to Ag-induced defect states, which can accelerate radiative recombination.

Ag-doped ZrS is synthesized using a variety of processes, including solid-state reaction, co-precipitation, and electrochemical deposition [16], [19]–[21], [22]–[30]. The advantages of each process can influence the material's final qualities. Electrochemical deposition gives fine control over doping concentration and homogeneity, which is critical for achieving desired electrical and optical properties. The exploration of Ag-doped ZrS materials has risen as they have advanced in many applications [18], [31], [32]. Optoelectronics researchers are investigating their advantageous bandgap and luminescence features for usage in LEDs and laser diodes. Their increased electrical conductivity makes them potential candidates for solid-state batteries and other electronic components. ZrS doped with Ag is a material system with superior characteristics for a variety of applications [17], [20], [21], [33], [34]. The incorporation of Ag into ZrS is projected to accelerate significantly the development of future electrical and optoelectronic products.

We intend to take advantage of silver doping's benefits to create a diverse and high-performance material for advanced technology applications. Silver doping in ZrS results in unique electronic and structural alterations, a property not seen in other materials with similar modifications. Merging ZrS's

intrinsic qualities with Ag creates a synergy, boosting performance beyond the capabilities of either material individually. These findings open new possibilities for ZrS-based materials in optoelectronics, thermoelectric, photovoltaics, and catalysis, broadening their potential uses. This study contributes significantly to our knowledge of doped chalcogenides due to the limited existing research on Ag-doped ZrS.

The study explores the improved optoelectronic properties of Ag-doped ZrS using electrochemical deposition, analyzing the optical, structural, and morphological features of the synthesized material.

II. Experimental Procedure

A. Material

The reagents used for the synthesis are zirconium (IV) oxychloride octahydrate ($ZrOCl_2.8H_2O$), thioacetamide (C_2H_5NS), silver nitrate ($AgNO_3$), Acetone, hydrochloric acid (HCl), distilled water, Carbon electrode, Fluorine doped tin oxide as substrate (FTO), Potentiostat which supplies a DC voltage in a two-electrode cell setup.

B. Preparation of FTO substrate

A 15-minute cleaning process, including ultrasonic baths and various cleaning agents, was applied to the FTO before deposition. An electric thermostatic oven dried the FTO at 65 °C for a specific duration. FTO's wide band gap makes it highly transparent in the visible light range, making it perfect for solar cells and optoelectronic devices. The material's high conductivity, achieved through oxygen vacancies and fluorine doping, creates a low electrical resistance when used as a substrate. FTO's chemical stability makes it more reliable in a variety of experimental circumstances than other conducting glasses. The FTO-immersed area measured approximately 2.5 cm2. The FTO's resistivity measures 15.5 ohm/square. ZrS and Ag-doped ZrS were used to coat the FTO substrate.

C. Synthesis of ZrS and Ag-doped ZrS material

A solution with 0.01 M concentration and 10 ml volume is mixed with zirconium (IV) oxychloride octahydrate ($ZrOCl_2.8H_2O)nSO_4$, thioacetamide (C_2H_5NS), and silver nitrate ($AgNO_3$), ranging from 0.02 in a 20/25 ml electrolyte solution. ZrS and Ag-doped ZrS material were subjected to ECD analysis. Fig. 1 illustrates the ECD setup, which comprises a DC power supply connected to a three-electrode cell. At room temperature, the deposition stayed the same for 5 seconds with a voltage of 10 V and pH of 5.6 in every experiment. Testing was conducted on the synthesized ZrS and Ag-doped ZrS material, with controlled parameters in place. A potential of 10 V was applied for deposition in a 50 ml beaker containing solvents for the undoped sample. By optimizing the deposition voltage from 10 to 14 V, the electrochemical bath was successfully established. 10 ml of precursors and 5 ml of the dopant precursor were added to the bath system. When the films were heated to 120 °C for 45 minutes, the tension of the material dissipated. The films' structural properties were analyzed using a Bruker D8-Advance X-ray diffractometer and Cu-Kα radiation (ʎ = 1.5406 Å) in continuous-scan mode. MIRA3 TESCAN scanning electron microscopy was used to analyze the film's surface morphology. The 756S UV-visible spectrophotometer was utilized to measure optical material wavelength, spanning from 300 to 1100 nm. The absorbance values were analyzed through optical spectral analysis to determine the optical and solid-state properties of the films. By employing the Jandel four-point probes method, we investigated their electrical characteristics.

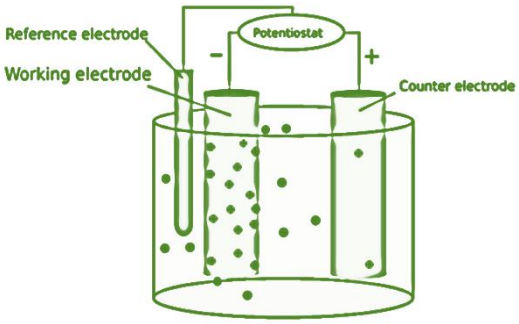

Fig. 1. Schematic diagram of electrochemical deposition technique (ECD).

III. Publication Principles

A. Optical study of ZrS and Ag-doped ZrS material

The absorbance of ZrS and Ag-doped ZrS is affected by the voltage applied, with higher voltage boosting carrier concentration and mobility, resulting in improved absorption properties. Changes in voltage (10 V, 12 V, and 14 V) impact how charges are distributed and the electric fields in the materials, leading to changes in their optical properties, as shown in the absorbance data in Fig. 2 (a). Silver (Ag) doping in ZrS leads to the generation of supplementary energy levels within the bandgap, promoting novel electronic transitions. Incorporating Ag decreases absorbance, resulting in more material absorbing light at shorter wavelengths. The absorption spectrum is altered by the presence of Ag through localized states [5], [6], [9], [35]–[37]. Enhance the total absorbance by increasing interactions between the dopant and the host lattice. At a voltage of 10 V, the absorbance reflects a baseline pattern, indicating the dominance of ZrS's inherent characteristics. Enhancement was noticed in Ag-doped ZrS, although not fully optimized. As voltage goes up, the electric field intensifies, resulting in improved charge separation and potentially a significant rise in absorbance for both materials.

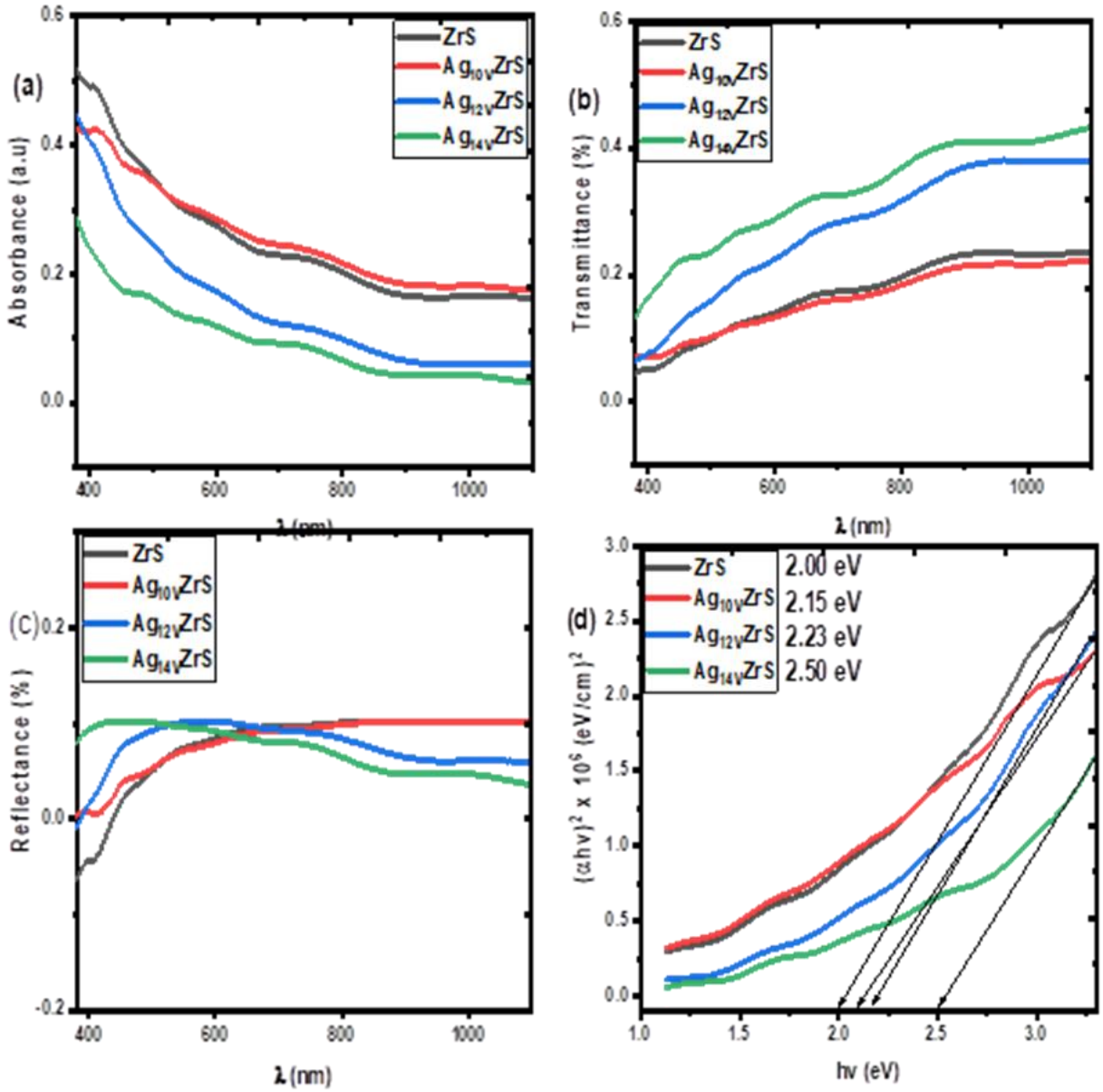

Fig. 2. (a) Absorbance (b) transmittance (c) reflectance, and (d) bandgap energy of ZrS and Ag-doped ZrS.

The presence of the Ag dopant causes more notable changes in the doped sample [5], [6], [9], [35]–[37]. At 14 V, the absorbance peaks as charge carriers exhibit their highest mobility and interaction. The addition of Ag to ZrS leads to a broader absorption spectrum or increased peaks, demonstrating enhanced optical properties.

Fig. 2 (b) illustrates how the transmittance of ZrS and Ag-doped ZrS changes at various voltages, indicating a significant impact of silver incorporation on the material's optical characteristics. The variations in the dielectric constant and band structure mainly caused the alteration resulting from doping. At voltage levels of 10 V, 12 V, and 14 V, the transmittance spectrum displays unique patterns, indicating that higher voltage levels impact the absorption and excitation of photons within the material. Increasing voltage enhances the excitation of electrons, leading to a potential rise in transmittance by encouraging electron movement between bands. The transmittance decreases at 10 V because there is less stimulation of charge carriers. Anticipate a slight rise in transmittance as additional electrons reach the energy for bandgap transition. A boost in transmittance may happen at 14 V, potentially resulting in saturation effects that increase the material's conductivity and improve light transmission [5], [6], [9], [35]–[37]. Silver atoms produce specific states that help electron shifts. The existence of these states boosts optical absorption and transmittance at particular energy levels. The

transmittance of Ag-doped ZrS is higher at particular voltages than that of ZrS, thanks to the doping effects that change the electronic structure.

The reflectance of ZrS and Ag-doped ZrS changes at different voltage conditions (10 V, 12 V, and 14 V) mainly because of variations in electronic properties like band structure and optical absorption. These variables are critical in influencing the reflectance levels presented in Fig. 2 (c). The doping effects alter carrier concentration and energy levels, leading to this behaviour. The reflectance of ZrS and Ag-doped ZrS changes with voltage conditions (10 V, 12 V, and 14 V) mainly because of shifts in electronic characteristics like band structure and optical absorption, which play a crucial role in reflectance determination. The doping effects are responsible for this behaviour by altering carrier concentration and energy levels. The application of voltage leads to the creation of an electric field that affects the distribution and mobility of charge carriers. Increasing voltage boosts the electric field, enhancing charge carrier movement and conductivity, potentially modifying reflectance [5], [6], [9], [35]–[37]. Reflectance is low because carrier activation is limited. The inherent qualities of ZrS prevail, causing a rise in absorption and a drop in reflectance. Reflectance increases as voltage goes up. By increasing the electric field, carrier mobility is enhanced, causing absorption to decrease and reflectance to increase. Reflectance continues to rise as the electric field boosts carrier mobility and changes the optical reaction. The enhanced doping effect of silver can result in a notable boost in reflectance, thanks to better conductivity and decreased absorption. The presence of Ag leads to the formation of localized states in the band structure, aiding in the creation of carriers. This results in more free carriers boosting reflectance, especially at higher voltages, when the material shifts from being more insulating to more conductive. The scattering of light is altered by doped materials, leading to shifts in reflectance.

ZrS has a bandgap energy of 2.00 eV, hinting at its semiconductor potential. Fig. 2 (d) shows that Ag-doped ZrS has higher bandgap energies ranging from 2.15 eV to 2.50 eV, indicating changes in its electronic properties from doping [5], [6], [9], [35]–[37]. The higher bandgap energy in Ag-doped ZrS leads to enhanced confinement of charge carriers, benefiting electronic applications for better efficiency and performance. ZrS is classified as a semiconductor, making it ideal for optoelectronics and photovoltaic uses. Its 2.00 eV bandgap enables the absorption of visible light, proving valuable for solar energy applications. The rise in bandgap energy due to Ag doping indicates a change in the ZrS electronic structure. Introducing extra energy levels or increasing lattice strain leads to higher bandgap energies (ranging from 2.15 eV to 2.50 eV), influencing electron mobility and energy transitions [5], [6], [9], [35]–[37]. The introduction of Ag creates additional energy levels in the band structure, causing the bandgap energy to rise. Useful for applications that need adjustable bandgaps.

The refractive index of a material shows the degree of light bending or refraction upon entry. Wavelength, voltages, and the material's composition, including dopants such as Ag in ZrS, play a role in its influence. The changes in refractive index result from variations in electron mobility and density within the material when voltages of 10, 12, and 14V are applied in Figure 3 (a). The addition of Ag to ZrS results in the presence of free carriers (electrons) in the material, influencing its optical characteristics. Ag's presence causes a shift in refractive index by boosting electron density, changing the material's interaction with light. Increasing the voltage boosts carrier concentration, which improves material conductivity and could change the refractive index. The alignment of dipoles in the material is altered by an applied electric field, causing shifts in its optical characteristics [5], [6], [9], [35]–[37]. The baseline value of the refractive index indicates the inherent characteristics of both ZrS and Ag-doped ZrS. An increase in carrier concentration from the applied voltage causes the refractive index to rise, resulting in improved light-matter interactions. The refractive index continues to rise to 14V as the electric field becomes stronger, possibly saturating when all carriers are stimulated. Ag-doped ZrS demonstrate a greater refractive index than pure ZrS under identical voltage conditions because of the extra free carriers. The increase in refractive index becomes more noticeable as the voltage rises in Ag-doped ZrS, indicating its heightened responsiveness to electrical activation.

The extinction coefficient indicates the light absorption of a material. Figure 3 (b) displays a consistent increase in ZrS and Ag-doped ZrS deposited at various voltages (10, 12, and 14V) across wavelengths from 310 nm to 1000 nm. This indicates that both materials improve in light absorption effectiveness with increased voltages. The excitation of electrons in ZrS is minimal at this reduced voltage, leading to a lower extinction coefficient. The material mainly absorbs light within certain energy ranges linked to its bandgap. Silver doping in ZrS with Ag creates localized states in the band structure, potentially boosting the extinction coefficient compared to undoped ZrS due to increased absorption at specific photon energy [5], [6], [9], [35]–[37]. Boosting the voltage increases the stimulation of charge carriers, resulting in a higher extinction coefficient for both ZrS and Ag-doped ZrS. The higher energy level enables additional electrons to transition to higher states, resulting in the absorption of more light. The addition of Ag-doping can enhance absorption by introducing extra electronic states, which results in a more prominent peak in the extinction coefficient spectrum. The material is experiencing increased excitation at 14 V. The extinction coefficient reaches a maximum due to the saturation of absorption processes, where most of the available electronic states are being utilized for light absorption [5], [6], [9], [35]–[37]. The increased conductivity and absorption properties of Ag-doped ZrS result in a much higher extinction coefficient when compared to ZrS, suggesting more effective light absorption.

The optical conductivity of ZrS and Ag-doped ZrS changes with applied voltage, leading to notable differences in absorption and reflection characteristics at various voltages, impacting its electronic transitions in Figure 3 (c). The optical conductivity of ZrS is enhanced by doping Ag, causing shifts in absorption peaks and overall conductivity improvements from the electronic structure changes [5], [6], [9], [35]–[37]. At voltages of 10 V, 12 V, and 14 V, the optical properties exhibit a clear voltage dependence, suggesting adjustable electronic properties ideal for diverse optoelectronic device applications.

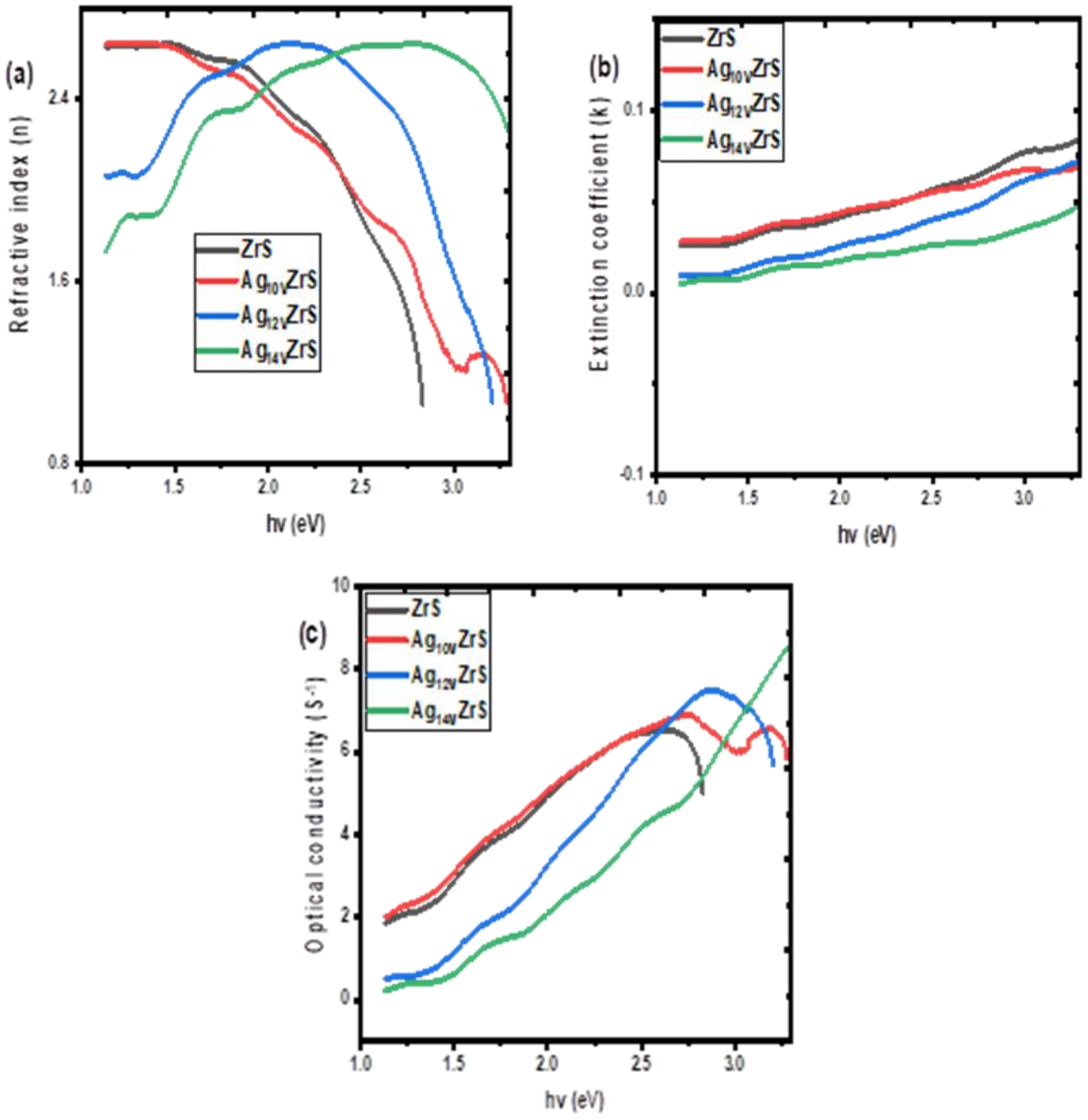

Fig. 3. (a) Refractive index (b) extinction coefficient, and (c) optical conductivity of ZrS and Ag-doped ZrS.

The real dielectric constant (ε′) shows how well a material can store electrical energy with an electric field. At different voltages (10 V, 12 V, and 14 V), the value fluctuates for ZrS and Ag-doped ZrS owing to shifts in charge distribution and polarization effects. The imaginary dielectric constant (ε″) represents the energy dissipation in the material because of absorbing electromagnetic energy [5], [6], [9], [35]–[37]. The differences in ε″ at the specified voltages provide an understanding of dissipation mechanisms in ZrS and Ag-doped ZrS in Fig. 3(a) and (b). Materials exhibit significant

changes in dielectric properties when voltage is applied. Increasing the voltage from 10V to 14V enhances polarization effects in both ZrS and Ag-doped ZrS, leading to changes in real and imaginary dielectric constants. At voltage levels of 10V, 12V, and 14V, the actual dielectric constant of ZrS rises because of increased polarization phenomena [5], [6], [9], [35]–[37]. As the voltage rises, more charge carriers align with the electric field, resulting in a higher ε′. The addition of silver (Ag) changes the carrier concentration and mobility, raising the real dielectric constant compared to ZrS. Doping increases the number of charge carriers or changes the crystal structure, improving the material's polarization capacity.

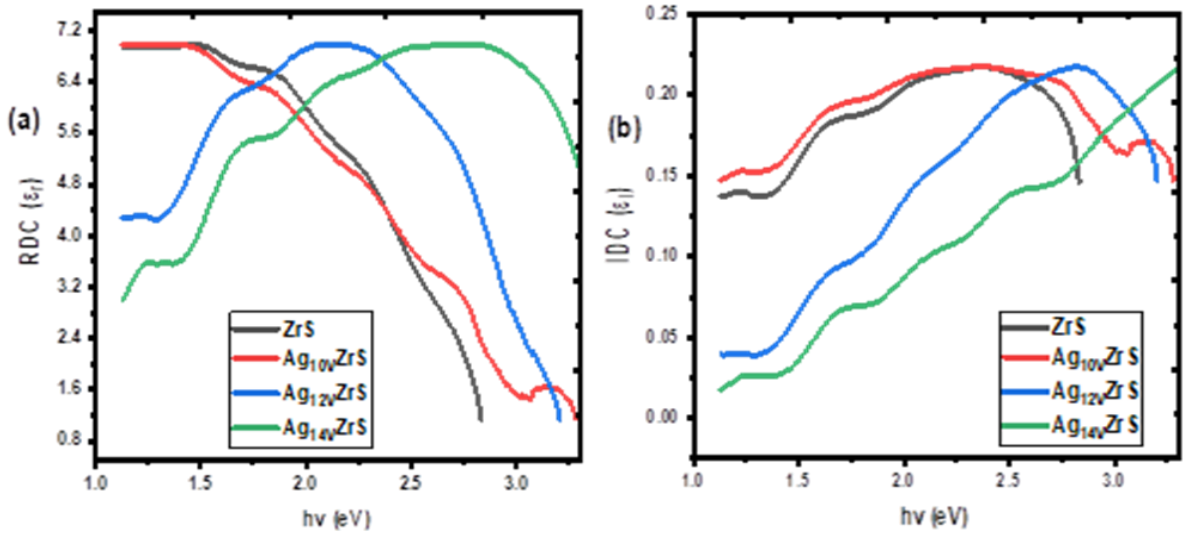

Fig. 4. (a) Real and (b) imaginary dielectric constant of ZrS and Ag-doped ZrS.

B. XRD study of ZrS and silver-doped ZrS

Fig. 5 depicts the X-ray diffraction (XRD) patterns of ZrS and Ag-doped ZrS. The crystal planes of 101, 103, 111, and 112 are identified by precise 2θ angles of 23.59°, 34.91°, 48.42°, and 62.62° for ZrS and 19.64°, 33.61°, 44.48°, and 63.31° for Ag-doped ZrS. Applying different voltages (10, 12, 14 V) changes the electrical structure, affecting peak positions and intensities in XRD examination. Doping and voltage changes cause adjustments in material characteristics. The strong peaks' intensity corresponds to the sample's crystallinity and purity [1], [38]–[45]. Distinct peaks suggest organized crystal arrangements. The peaks indicate the formation of a new phase or a shift in the crystal structure because of silver doping. The shift in peak positions relative to ZrS implies changes in lattice characteristics, caused by the addition of Ag ions in the ZrS lattice. The application of different voltages impacts how crystals nucleate and develop during synthesis. Increased voltages result in increased energy levels, which affect ion mobility and may cause larger or more crystalline formations [1], [38]–[45]. A rise in voltage causes a higher peak intensity, indicating improved crystallinity, as well as a drop in peak width, implying smaller particle sizes and greater order. In contrast, an excess voltage can induce defects and strain, broadening peaks and decreasing intensity. Introducing Ag resulted in a drop in specific peak intensities or changes in peak positions, indicating structural modifications. By comparing the XRD patterns of ZrS and Ag-doped ZrS, we may learn about their interaction, which may affect electrical characteristics and stability. Table I show the structural parameters of ZrS and Ag-doped ZrS.

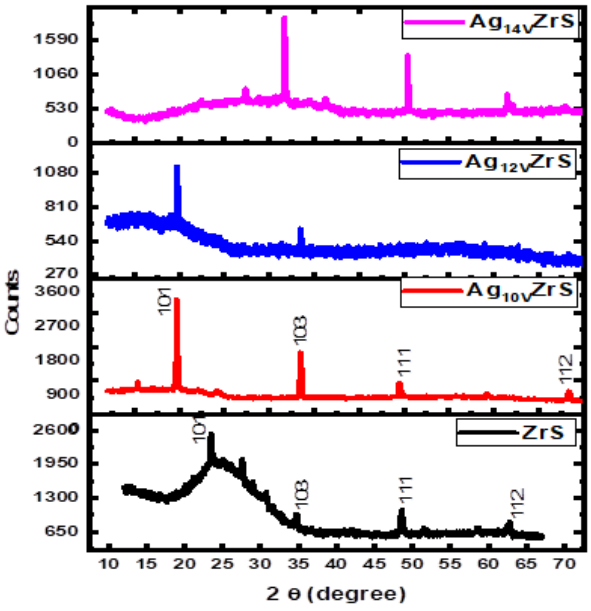

Fig. 5. XRD pattern of ZrS and Ag-doped ZrS.

Table I. Structural parameters of ZrS and Ag-doped ZrS.

Sample	2θ (°)	d (spacing) (Å)	Lattice constant (Å)	(β) FWHM	(hkl)	Grain Size (D) (nm)	Dislocation density, σ (lines/m^2)
ZrS	23.5941	3.7672	6.5250	0.2021	101	7.0076	6.2032
	34.9137	2.5674	5.1349	0.2021	103	7.1908	5.8912
	48.4287	1.8778	3.7557	0.2021	111	7.5215	5.3847
	62.6298	1.4819	3.3136	0.2021	112	8.0295	4.7250
Ag_{10V}/ZrS	19.6493	4.5137	7.8180	0.3323	101	4.2346	1.6987
	33.6103	2.6639	5.3279	0.3323	103	4.3587	1.6034
	44.4841	2.0347	4.0695	0.3323	111	4.5080	1.4989
	63.3185	1.4674	3.2812	0.3323	112	4.9022	1.2676
Ag_{12V}/ZrS	19.6493	4.5137	7.8180	0.3411	101	4.1254	1.7898
	33.6103	2.6639	5.3279	0.3411	103	4.2462	1.6894
	44.4841	2.0347	4.0695	0.3411	111	4.3917	1.5794
	63.3185	1.4674	3.2812	0.3411	112	4.7757	1.3356
Ag_{14V}/ZrS	19.6493	4.5137	7.8180	0.3501	101	4.0193	1.8855
	33.6103	2.6639	5.3279	0.3501	103	4.1371	1.7797
	44.4841	2.0347	4.0695	0.3501	111	4.2788	1.6638
	63.3185	1.4674	3.2812	0.3501	112	4.6530	1.4070

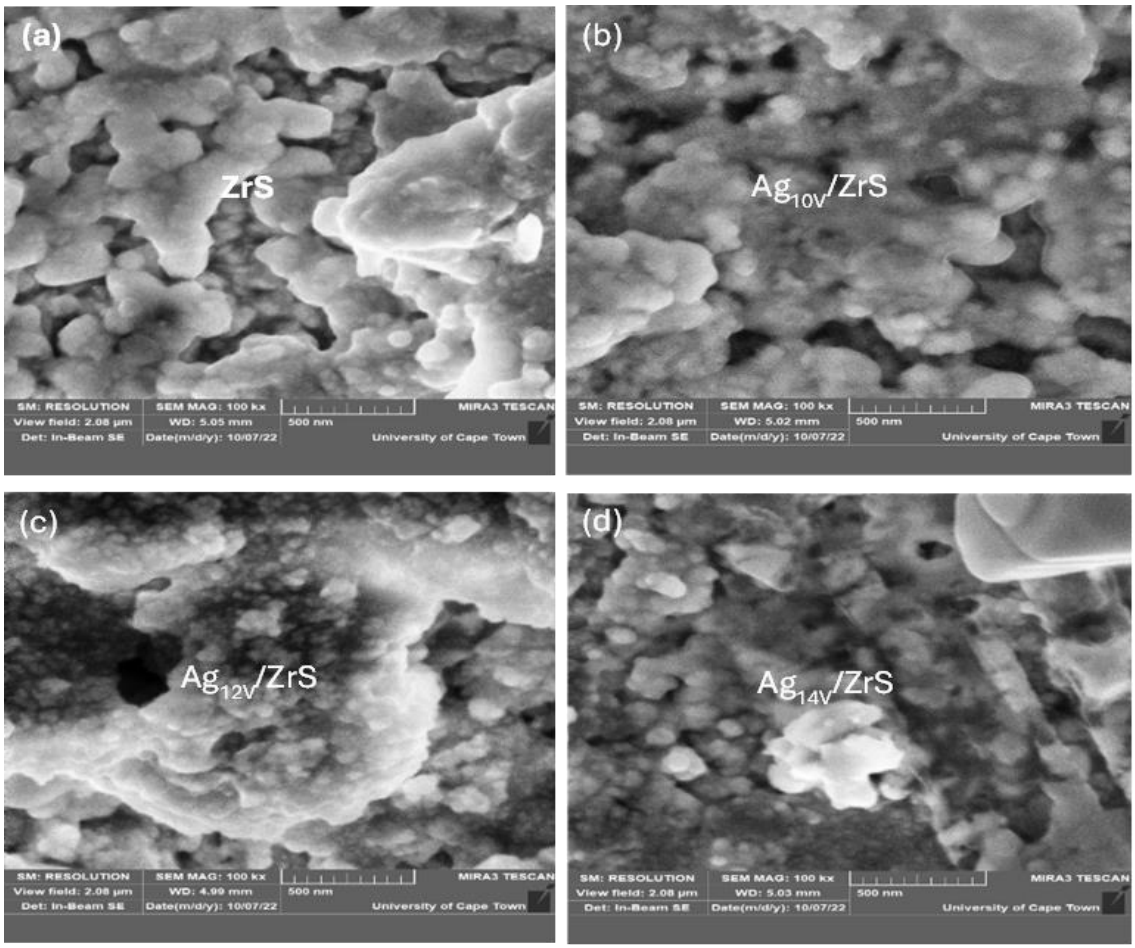

Fig. 6. Surface micrograph of (a) ZrS and Ag doped ZrS at (b) 10 V (c) 12 V, and (d) 14 V.

C. *Surface morphology of ZrS and silver-doped ZrS*

Fig. 6 depicts the surface morphology of ZrS and Ag-doped ZrS deposited at different deposition voltages. As the voltage increases from 10 V to 14 V, the morphology changes, indicating textural variations and potentially detectable densities inside ZrS and Ag-doped material. Doping with Ag alters the surface morphology of ZrS, resulting in increased grain size. ZrS has a smooth surface with modest grain sizes.

Reduced energy levels cause lower kinetic energy in the atoms being deposited, resulting in reduced nucleation [1], [38]–[45]. Increasing the voltage to 10 V causes the atoms to gain kinetic energy, which increases surface roughness. This results in larger grains and a textured surface, indicating improved nucleation and growth dynamics. Below 12 V, the surface appearance exhibits significant characteristics, such as increased particle size and clustering. High energy levels allow atoms to move freely, leading small grains to merge into bigger ones. The introduction of Ag at this lower voltage level results in a more consistent dispersion of Ag particles while keeping the surface smooth. The interaction between Ag and ZrS causes localized morphological alterations. As the voltage increases, Ag raises surface roughness more than undoped ZrS. The silver atoms act as starting points, stimulating the formation of larger and more evenly distributed grains [1], [38]–[45]. At 14 V, the Ag-doped ZrS exhibits noticeable morphological changes, such as increased grain size and surface features. Increased energy levels make Ag more effectively absorbed into the ZrS structure, improving its electrical and optical properties. Increased voltages are connected to higher crystallinity because they increase atomic mobility, resulting in better arrangement and fewer defects in the crystal structure. However, an excess of energy might result in faults or dislocations, particularly in Ag-doped materials. EDX is used to determine the elemental composition of both ZrS and Ag-doped ZrS. ZrS is composed of zirconium (Zr) and sulfur (S), and it has a layered structure that improves its semiconductor properties (Figure 7). The covalent connection between Zr and S produces unusual electrical characteristics [1], [38]–[45]. Ag-doped ZrS contains silver (Ag) atoms injected into its lattice. The doping level varies, affecting the total composition. The use of Ag in doping increases the number of charge carriers, which improves conductivity.

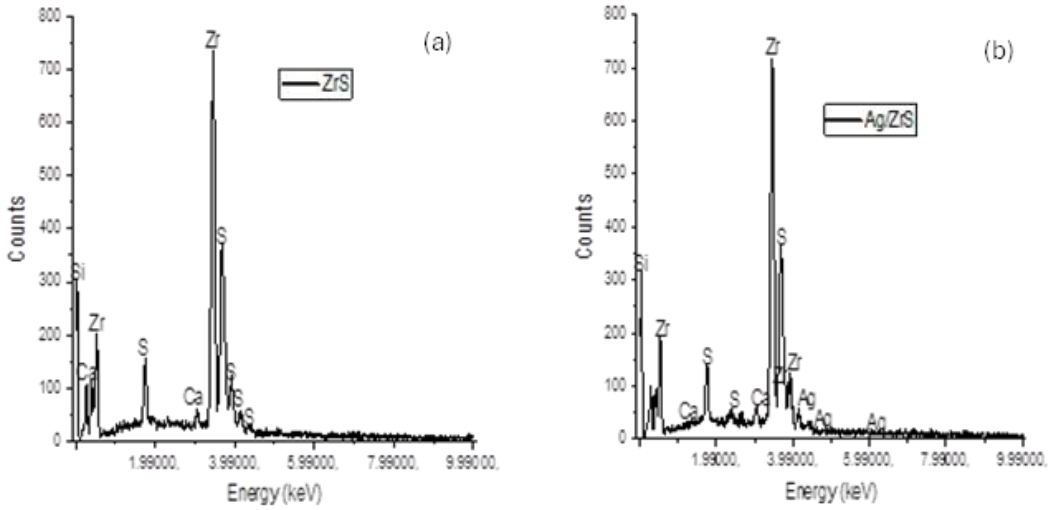

Fig. 7. EDX of (a) ZrS, and (b) Ag-doped ZrS.

D. *Electrical study of ZrS and silver-doped ZrS*

Table II and Fig. 8 show the thickness measurements of ZrS and ZrS doped with silver (121.32, 129.09, 121.00, 123.01 nm), which demonstrate the impact of voltage on material structure and its impacts on performance via density and crystal quality.

Table II. Electrical properties of ZrS and silver doped ZrS.

Samples	Thickness, t (nm)	Resistivity, ρ (Ωm)	Conductivity, σ (S/m)
ZrS	121.32	2.36×10^6	4.34×10^5
Ag $_{10V}$/ZrS	129.09	2.18×10^6	4.58×10^5
Ag $_{12V}$/ZrS	121.00	2.12×10^6	4.71×10^5
Ag $_{14V}$/ZrS	123.01	2.09×10^6	4.78×10^5

The resistivity values (2.36, 2.18, 2.12, 2.09 Ω.m) decrease with increasing voltage, indicating greater conduction and a higher charge carrier concentration [1], [38]–[45]. The increasing conductivity values (4.34, 4.58, 4.71, 4.78 S/m) indicate that increased voltage leads to improved conductivity, which is beneficial for applications that require effective charge transfer. At higher voltages, an ideal level of Ag doping in ZrS is assumed. As the voltage increases, the resistivity drops, indicating that the material's resistance reduces with voltage. The trend implies increased charge carrier mobility, which is attributed to improved dopant ionization or charge transport processes. Higher voltages are preferable in electronic devices because they reduce resistance, indicating increased conductivity. The conductivity increases as the voltage increases, indicating that the material is getting more efficient at conducting electricity [1], [38]–[45]. Increased conductivity values suggest that Ag doping enhances ZrS electrical characteristics by providing more charge carriers. The constant increase in conductivity corresponds to the decrease in resistance, reinforcing the idea that higher voltages

improve charge transport. The thickness remains largely constant, indicating consistent material quality. Increasing the voltage improves both resistivity and conductivity, illustrating the favourable effect of voltage on the electrical properties of Ag-doped ZrS [1], [38]–[45]. These findings suggest that adding silver increases the capabilities of ZrS, making it a viable option for applications requiring excellent electrical conductivity, such as sensors, transistors, and solar panels.

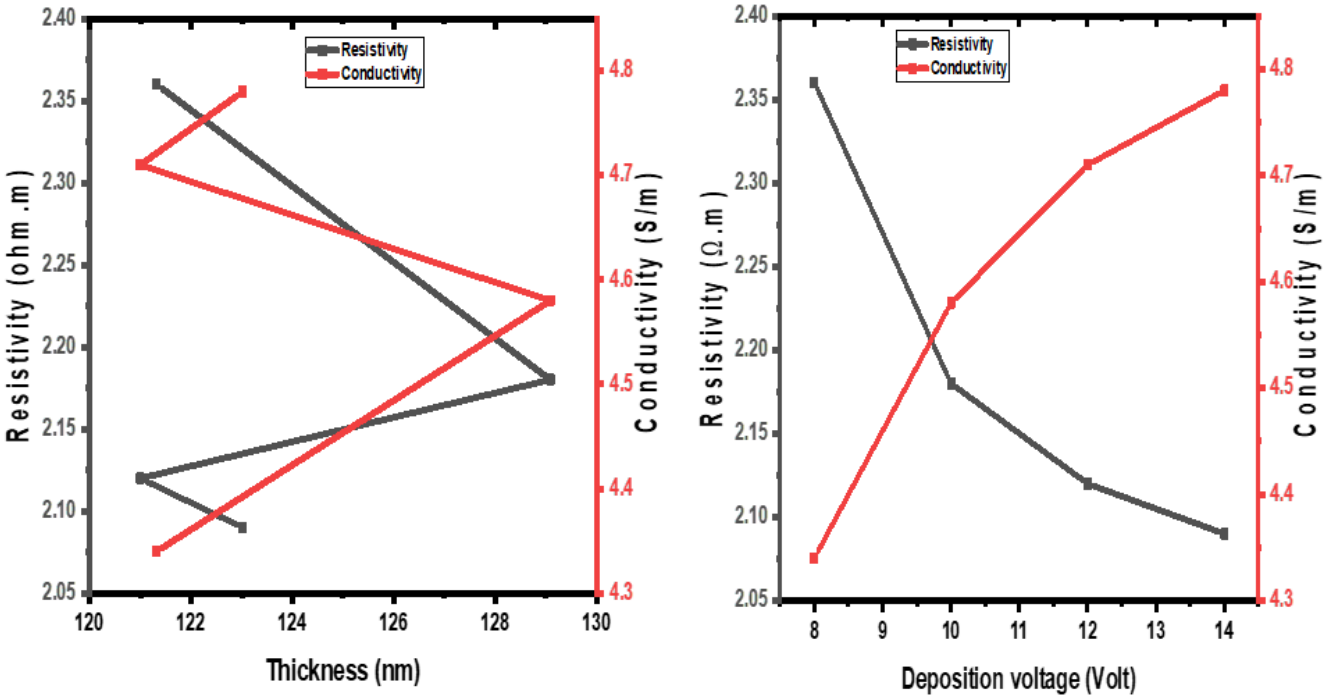

Fig. 8. Resistivity and conductivity of (a) ZrS, and (b) Ag-dopedAg-doped ZrS.

IV. Conclusion

The electrochemical deposition technique was successfully used to deposit ZrS and Ag-doped ZrS by varying the deposition voltage. The crystal orientations of 101, 103, 111, and 112 can be distinguished by specific 2θ angles of 23.59°, 34.91°, 48.42°, and 62.62° in ZrS and 19.64°, 33.61°, 44.48°, and 63.31° in Ag-doped ZrS. Adjusting voltages (10, 12, 14V) can affect the electrical configuration in XRD analysis, thus influencing peak positions and intensities. Incorporating Ag at this lower voltage setting results in a more even dispersion of Ag particles without affecting the surface's smoothness. Localized morphological alterations occur when Ag and ZrS interact with each other. As voltage rises, the absorbance of ZrS and Ag-doped ZrS changes with the applied voltage, enhancing carrier concentration and mobility at higher voltages to enhance absorption properties. At voltage levels of 10V, 12V, and 14V, the transmittance spectrum displays unique patterns, indicating that higher voltage levels impact the absorption and excitation of photons within the material. Increasing voltage enhances the excitation of electrons, leading to a potential rise in transmittance by encouraging electron movement between bands. The transmittance decreases at 10 V because there is less stimulation of charge carriers. ZrS displays a bandgap energy of 2.00 eV, showing its potential as a semiconductor material and doping Ag in ZrS results in higher bandgap energies between 2.15 eV and 2.50 eV, leading to modifications in its electronic characteristics. Ag increases surface roughness more compared to ZrS without doping. The resistivity values decrease as the voltage increases, suggesting enhanced conduction and more charge carriers. The rising conductivity values (4.34, 4.58, 4.71, 4.78) (S/m) suggest that higher voltage enhances conductivity, benefiting applications needing efficient charge transfer.

Authors Contribution Statement

Shaka O Samuel, Ernest O Ojegu and Imosobomeh L Ikhioya: methodology, conceptualization, data curation, data collection, Ernest O Ojegu, Imosobomeh L Ikhioya: samples characterization, first-draft writing, software, reviewing, and editing. Imosobomeh L Ikhioya, Shaka O Samuel: supervisor, investigation and visualization.

Availability of Data

Data can be accessed upon request.

References

[1] R. O. Ijeh, A. C. Nwanya, A. C. Nkele, I. G. Madiba, A. K. H. Bashir, A. B. C. Ekwealor, R. U. Osuji, M. Maaza, and F. Ezema, "Optical, electrical and magnetic properties of copper doped electrodeposited MoO_3 thin films. Ceramics Inter., vol. 46, no. 8, pp. 10820–10828, 2020. https://doi.org/10.1016/j.ceramint.2020.01.093.

[2] A. I. Agbrara, E. O. Ojegu, M. O. Osiele, and I. L. Ikhioya, "Electrochemically Synthesize SrSe/ZrSe Heterostructure Material for Photovoltaic Application," Adv. J. of Chem. Sect. A, vol. 6, no. 4, pp. 401–411, 2023, doi: 10.48309/AJCA.2023.407032.1385.

[3] L. F. Jiang, W. Z. Shen, and H. Z. Wu, "Optical properties of SrSe thin films grown by molecular beam epitaxy," J. of App. Phy., vol. 91, no. 11, pp. 9015–9018, 2002, doi: 10.1063/1.1474593.

[4] S. M. Mousavi, J. B. Raoof, and M. Ghani, "Electrocatalysis of methanol at the surface of carbon paste electrode modified with composite of Cu-Al-layered double hydroxide and graphene oxide," J. of Iran. Chem. Soc., vol. 20, no. 9, pp. 2285–2295, 2023, doi: 10.1007/s13738-023-02836-4.

[5] Y. Tian, M. Zheng, Y. Cheng, Z. Yin, J. Jiang, G. Wang, J. Chen, X. Li, J. Qi, and X. Zhang, "Epitaxial growth of $ZrSe_2$ nanosheets on sapphire: Via chemical vapour deposition for optoelectronic application". J. of Mat. Chem. C, vol. 9., no. 39, pp. 13954–13962, 2021. . https://doi.org/10.1039/d1tc03339e.

[6] M. Wang, Y. Zheng, L. Guo, X. Chen, H. Zhang, and D. Li, "Nonlinear optical properties of zirconium diselenide and its ultra-fast modulator application," Nanomat., vol. 9, no. 10, pp. 1–12, 2019, doi: 10.3390/nano9101419.

[7] X. Zhou, K. H. L. Zhang, J. Xiong, J. H. Park, J. H. Dickerson, and W. He, "Size- and dimensionality-dependent optical, magnetic and magneto-optical properties of binary europium-based nanocrystals: EuX (X = O, S, Se, Te)," Nanotech., vol. 27, no. 19, 2016, doi: 10.1088/0957-4484/27/19/192001.

[8] R. Yue, A. T. Barton, H. Zhu, A. Azcatl, L. F. Pena, J. Wang, X. Peng, N. Lu, L. Cheng, P. Addou, S. McDonnell, L. Colombo, J. W. P. Hsu, J. Kim, M. J. Kim, R. M. Wallace and C. L. Hinkle, "$HfSe_2$ thin films: 2D transition metal dichalcogenides grown by molecular beam epitaxy". ACS Nano, vol. 9, no. 1, pp. 474–480, 2015. https://doi.org/10.1021/nn5056496.

[9] X, Zhao, H. Zhang, T. Chen, Y. Gao, H. Wang, T. Wang and S. Wei, "Modulating electronic and magnetic properties of monolayer $ZrSe_2$ by doping". Superlatt. & Microstruct., vol. 120, pp. 659–669, 2018. https://doi.org/10.1016/j.spmi.2018.06.038.

[10] H. Gleiter, "Nanostructured materials: basic concepts and microstructure," Acta Mater., vol. 48, no. 1, pp. 1–29, 2000, doi: 10.1016/S1359-6454(99)00285-2.

[11] P. Moriarty, "Nanostructured materials," Rep. Prog. Phy., vol. 64, no. 3, pp. 297–381, 2001, doi: 10.1088/0034-4885/64/3/201.

[12] F. Gao and E. Reichmanis, "Introduction: Emerging Materials for Optoelectronics," Chem. Rev., vol. 123, no. 18, pp. 10835–10837, 2023, doi: 10.1021/acs.chemrev.3c00349.

[13] F. Adams and C. Barbante, "Nanotechnology and Analytical Chemistry," Compr. Anal. Chem., vol. 69, pp. 125–157, 2015, doi: 10.1016/B978-0-444-63439-9.00004-9.

[14] S. Sweeney and A. Adams, "Optoelectronic Devices and Materials," Springer Handbooks, pp. 887–916, 2007, doi: 10.1007/978-0-387-29185-7_37.

[15] K. I. Udofia, I. L. Ikhioya, A. U. Agobi, D. N. Okoli, and A. J. Ekpunobi, "Effects of zirconium on electrochemically synthesized tin selenide materials on fluorine-doped tin oxide substrate for photovoltaic application," J. of Indian Chem. Soc., vol. 99, no. 10, 2022, doi: 10.1016/j.jics.2022.100737.

[16] K. Haribaaskar, K. S. Yoganand, T. V. Rajendran, and M. V. Arularasu, "Synthesis of Zr-doped CeO2 nanoparticles for photocatalytic degradation of methyl orange and electrochemical properties," Biomass Convers. Biorefinery, 2024, doi: 10.1007/s13399-024-05941-3.

[17] H. Mersian, M. Alizadeh, and N. Hadi, "Synthesis of zirconium doped copper oxide (CuO) nanoparticles by the Pechini route and investigation of their structural and antibacterial properties," Ceram. Int., vol. 44, no. 16, pp. 20399–20408, 2018, doi: 10.1016/j.ceramint.2018.08.033.

[18] P. Kaur, S. K. Chawla, S. S. Meena, S. M. Yusuf, and S. B. Narang, "Synthesis of Co-Zr doped nanocrystalline strontium hexaferrites by sol-gel auto-combustion route using sucrose as fuel and study of their structural, magnetic and electrical properties," Ceram. Int., vol. 42, no. 13, pp. 14475–14489, 2016, doi: 10.1016/j.ceramint.2016.06.053.

[19] S. O. Samuel, M. F. Lagbegha-ebi, E. P. Ogherohwo, and I. L. Ikhioya, "Improve physical properties of zirconium doped strontium sulphide for optoelectronic purpose," Results Opt., vol. 13, 2023, doi: 10.1016/j.rio.2023.100518.

[20] A. Khare, S. Mishra, D. S. Kshatri, and S. Tiwari, "Optical Properties of Rare Earth Doped SrS Phosphor: A Review," J. Elect. Mat., vol. 46, no. 2, pp. 687–708, 2017, doi: 10.1007/s11664-016-4988-1.

[21] S. Mishra, D. S. Kshatri, A. Khare, S. Tiwari, and P. K. Dwivedi, "SrS: Ce3+ thin films for electroluminescence device applications deposited by electron-beam evaporation deposition method," Mat. Lett., vol. 183, pp. 191–196, 2016, doi: 10.1016/j.matlet.2016.07.097.

[22] I. L. Ikhioya, I. Rufus, and N. I. Akpu, "Influence of temperature on energy band gap and other properties of undoped and cadmium doped manganese sulphide (MnS: Cd) synthesized for photovoltaic and optoelectronic application," Asian J. of Nanosci. Mat., vol. 5, no. 2, pp. 88–97, 2022, doi: 10.48309/JMNC.2022.2.1.

[23] I. L. Ikhioya, N. I. Akpu, E. U. Onoh, S. O. Aisida, I. Ahmad, M. Maaza, and F. Ifeanyichukwu, "Impact

of precursor temperature on physical properties of molybdenum doped nickel telluride metal chalcogenide material". Asian J. of Nanosci. & Orig. Res., vol. 2, pp. 156–167, 2023. https://doi.org/10.48309/JMNC.2023.2.5.

[24] I. L. Ikhioya and Okoli, "Electrochemical deposition of tin-doped zinc selenide (SnZnSe) thin film material," Asian J. Nanosci. Mat., vol. 3, no. 3, pp. 189–202, 2020, doi: 10.48309/JMNC.2020.3.3.

[25] E. N. Josephine, O. S. Ikponmwosa, and I. L. Ikhioya, "Enhanced physical properties of SnS / SnO semiconductor material," Asian J. Nanosci. Mat., vol. 3, pp. 199–212, 2023, doi: 10.48309/JMNC.2023.3.3.

[26] I. B. Okeoghenea, O. B. Uyoyou, and I. L. Ikhioya, "The influence of gamma irradiation 60Co On CoSe/Ag nanostructures material deposited via electrochemical deposition technique for photovoltaic application," Asian J. Nanosci. Mat., vol. 5, no. 1, pp. 11–21, 2022, doi: 10.48309/JMNC.2022.1.2.

[27] K. I. Udofia, I. L. Ikhioya, D. N. Okoli, and A. J. Ekpunobi, "Impact of doping on the physical properties of PbSe chalcogenide material for photovoltaic application," Asian J. Nanosci. Mat., vol. 6, no. 2, pp. 135–147, 2023, doi: 10.48309/JMNC.2023.2.3.

[28] I. L. Ikhioya, "Characterization of zinc sulphide thin film prepared by electrodeposition method," Int. J. Chem. Tech. Res., vol. 8, no. 2, 2015.

[29] I. L. Ikhioya, N. I. Akpu, and A. C. Nkele, "Influence of ytterbium (Yb) dopant on the optical properties of electrochemically deposited zinc oxide (ZnO) films," Mater. Res. Exp, vol. 8, no. 1, 2021, doi: 10.1088/2053-1591/abd5d6.

[30] I. L. Ikhioya, A. C. Nkele, S. N. Ezema, M. Maaza, and F. Ezema, "A study on the effects of varying concentrations on the properties of ytterbium-doped cobalt selenide thin films," Opt. Mat. (Amst)., vol. 101, 2020, doi: 10.1016/j.optmat.2020.109731.

[31] J. Ihanus, T. Hänninen, T. Hatanpää, T. Aaltonen, I. Mutikainen, T. Sajavaara, J. Keinonen, M. Ritala, and M. Leskelä, "Atomic layer deposition of SrS and BaS thin films using cyclopentadienyl precursors". Chem. of Mat., vol. 14, no. 5, pp. 1937–1944, 2002. https://doi.org/10.1021/cm0111130.

[32] P. R. Kharangarh, N. M. Ravindra, G. Singh, and S. Umapathy, "Synthesis and characterization of Nb-doped strontium cobaltite@GQD electrodes for high-performance supercapacitors," J. Energy Storage, vol. 55, 2022, doi: 10.1016/j.est.2022.105388.

[33] H. M. Saleh and A. I. Hassan, "Synthesis and Characterization of Nanomaterials for Application in Cost-Effective Electrochemical Devices," Sustain., vol. 15, no. 14, 2023, doi: 10.3390/su151410891.

[34] M. Sedighi, B. A. Nia, A. H. Hamad, and M. S. Othman, "Electronic and optical properties of Sr's nanosheet in 001 and 101 directions," Comp. Cond. Matt, vol. 22, 2020, doi: 10.1016/j.cocom.2019.e00445.

[35] A. P. V. Rakkini and K. Mohanraj, "Influence of pH of the electrolyte on the formation and properties of electrodeposited ZrSe2 thin films," Inorg. Nano-Metal Chem., vol. 52, no. 4, pp. 570–575, 2022, doi: 10.1080/24701556.2021.1913420.

[36] A. M. Sargar, N. S. Patil, S. R. Mane, S. N. Gawale, and P. N. Bhosale, "Electrochemical synthesis and characterisation of $ZrSe_2$ thin films," Int. J. Electrochem. Sci., vol. 4, no. 6, pp. 887–894, 2009, doi: 10.1016/s1452-3981(23)15192-3.

[37] M. Younis, M. Waqas, M. Awais, Y. Abbas, M. Mirza, M., Safdar and M. Tariq, "Biomolecule assisted hydrothermal synthesis of indium intercalated 2D $ZrSe_2$ microflowers for photocatalytic CO_2 reduction to MeOH and CH_4. Mat. Lett., vol. 309, 2022. https://doi.org/10.1016/j.matlet.2021.131368.

[38] I. L. Ikhioya, P. N. Okanigbuan, C. B. Agbakwuru, and B. U. Osolobri, "Journal of the Nigerian Association of Mathematical Physics © J . of NAMP Characterization of Zinc Sulphide / Cadmium Sulphide (ZnS / CdS) Superlattice by Electrodeposition Technique" J. Nig. Assoc. of Math. Phy., vol. 29, pp. 331–338, 2015.

[39] I. L. Ikhioya, A. C. Nkele, C. F. Okoro, C. O Obasi, G. M. Whyte, M. Maaza, and F. I. Ezema, "Effect of temperature on the morphological, structural and optical properties of electrodeposited Yb-doped $ZrSe_2$ thin films. Optik, vol. 220, 2020. https://doi.org/10.1016/j.ijleo.2020.165180.

[40] I. L. Ikhioya, S. O. Aisida, I. Ahmad, and F. I. Ezema, "The effect of molybdenum dopant on rare earth metal chalcogenide material," Chem. Phy. Impact, vol. 7, no. April, pp. 100269, 2023, doi: 10.1016/j.chphi.2023.100269.

[41] L. I. Ikhioya, U. K. Chime, C. F. Okoro, C. Iroegbu, M. Maaza, and F. I. Ezema, "Influence of dopant concentration on the electronic band gap energy of Yb-ZrSe2 thin films for photovoltaic application via electrochemical deposition technique," Mat. Res. Exp., vol. 7, no. 2, 2020, doi: 10.1088/2053-1591/ab7690.

[42] K. Nikonov, N. Ehlen, B. Senkovskiy, N. Saigal, A. Fedorov, A. Nefedov, C. Wöll, G. Di Santo, L. Petaccia and A. Grüneis, "Synthesis and spectroscopic characterization of alkali-metal intercalated $ZrSe_2$". Dalton Trans., vol. 47, no. 9, pp. 2986–2991, 2018. https://doi.org/10.1039/c7dt03756b.

[43] Z. Muhammad, M. W. Ali, I. A. Mir, Q. U. Khan, and L. Zhu, "Copper-doped induced ferromagnetic half-metal zirconium diselenide single crystals," Nanotech., vol. 31, no. 23, 2020, doi: 10.1088/1361-6528/ab72b3.

[44] X. Pang, R. Wang, X. Che, and F. Huang, "$SrZnSnSe_4$: Synthesis, crystal structure and nonlinear optical properties," J. Solid State Chem., vol. 297, 2021, doi: 10.1016/j.jssc.2021.122092.

[45] I. L. Ikhioya, A. Nawal, E. O. Stanley, C. I. David and N. O. Ruth, "Synergistic effects of gadolinium oxide into the matrix of zeolitic imidazolate frameworks (ZIFs) for supercapacitor applications". Chem. of Inorg. Mat., 100075, 2024. https://doi.org/10.1016/j.cinorg.2024.100075.